Optomechanically Induced Birefringence and Optomechanically Induced Faraday Effect

Robert Duggan,[1,*] Javier del Pino,[2,*] Ewold Verhagen,[2] and Andrea Alù[1,3,4,5,†]
[1]Department of Electrical and Computer Engineering, The University of Texas at Austin, Austin, Texas 78712, USA
[2]Center for Nanophotonics, AMOLF, Science Park 104, 1098 XG Amsterdam, The Netherlands
[3]Photonics Initiative, Advanced Science Research Center, City University of New York, New York 10031, USA
[4]Physics Program, Graduate Center, City University of New York, New York 10016, USA
[5]Department of Electrical Engineering, City College of The City University of New York, New York 10031, USA

(Received 1 April 2019; published 9 July 2019)

We demonstrate an optomechanical platform where optical mode conversion mediated by mechanical motion enables the arbitrary tailoring of polarization states of propagating light fields. Optomechanical interactions are realized in a Fabry-Pérot resonator, which naturally supports two polarization-degenerate states while an optical control field induces rotational symmetry breaking. Applying such principles, the entire Poincaré sphere is spanned by just optical control of the driving field, realizing reciprocal and nonreciprocal optomechanically induced birefringence for linearly polarized and circularly polarized control driving. A straightforward extension of this setup also enables all-optical tunable isolation and circulation. Our findings open new avenues to exploit optomechanics for the arbitrary manipulation of light polarization.

DOI: 10.1103/PhysRevLett.123.023602

The generation of arbitrary light polarization states is of major fundamental and technological relevance in nonlinear and quantum optics [1], communication networks [2], and microscopy [3,4]. Reciprocal and nonreciprocal polarization control is conventionally attained in bulk optics by wave plates and Faraday rotators, respectively, which rely on anisotropic or magnetically biased materials to induce birefringence. Both effects are intrinsically weak in bulk materials, requiring sizable driving fields and structures larger than the wavelength. More recently, engineered metasurfaces [5–8] have been developed to overcome these limitations across the electromagnetic spectrum, with tunability enabled by both electric [9] and magnetic [10,11] biasing. Polarization rotation is nevertheless limited in these structures. While a few platforms [12,13] have been recently proposed to provide complete tunability of the polarization state in a compact structure, they are characterized by complex implementations and modulation schemes.

Optomechanical technologies exploit sharp photonic resonances coupled to mechanical modes to enable a new degree of control over light, examples of which are the swapping of photons into phonons and back [14–17] and optomechanically induced transparency [18,19]. In this context, multimode systems have been recognized for their potential to convert photons from one cavity mode to another one via mechanical excitations. This additional degree of control over light allows quantum and classical applications, such as wavelength conversion between two distant optical frequencies [20–23] that can feature adiabatic quantum state transfer [24,25], nondemolition measurements [26], entanglement generation [27–29], nonreciprocal transport, and optical routing [30–34]. For the large part, these proposals have been based on manipulating the scalar properties of photons, while their vector nature has been only recently pinpointed [35–37].

In this Letter, we demonstrate how optomechanically induced mode conversion enables the arbitrary control of optical polarization. For simplicity and clarity of presentation, we focus on a canonical optomechanical system, consisting of a high-Q planar Fabry-Pérot resonator with a movable mirror, as is used in many experiments (see Fig. 1), but the analysis is valid for any system hosting degenerate modes of orthogonal polarization that are both coupled to a mechanical resonator mode [36,38–48]. Similar concepts may be envisioned in a broad class of 2D and 3D geometries. Optical pumping in a particular polarization state breaks rotational symmetry and induces a tunable linear interaction between different polarizations. In contrast to static radiation-pressure-induced chirality in prepatterned metasurfaces [49], our approach exploits dynamical backaction effects and coherent mode conversion for fully tunable and efficient polarization control. Indeed, by bringing ideas of coherent polarization manipulation via electromagnetically induced transparency in atoms [50] into the realm of linear optomechanics, we allow a rich regime of reciprocal and nonreciprocal interactions permitting tunable all-optical isolation and circulation.

Our model includes two degenerate electromagnetic modes with equal frequencies ω_{cav}, decay rates κ, and annihilation operators $\hat{\mathbf{a}}^T = (\hat{a}_H, \hat{a}_V)$ (H and V label

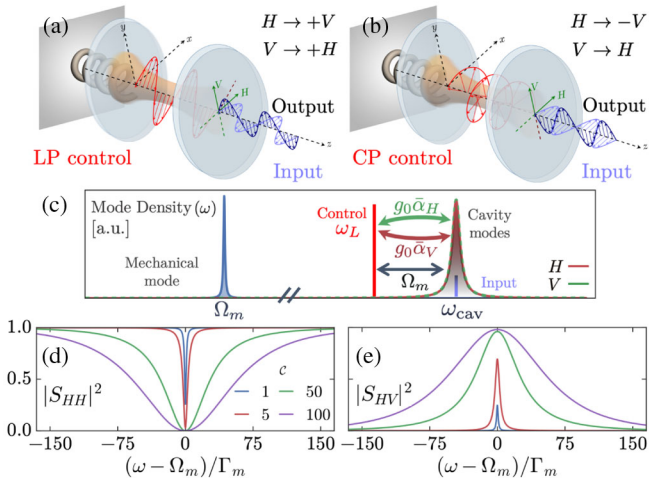

FIG. 1. (a),(b) Sketch of the proposed geometry. A pump field (red) induces coupling between two degenerate cavity modes with orthogonal polarizations, altering the polarization state of a probe (blue) upon reflection (black). (c) Schematic of the relevant frequencies and resonances. A red-detuned control field (ω_L) couples to a weak probe signal near the cavity resonance ($\omega_{\rm cav}$) through a mechanical mode (Ω_m). Lower panels show the reflectivity spectra for H-polarized input into the H and V output channels. The output is reciprocal ($\mathcal{S}_{HV}=\mathcal{S}_{VH}$) for a linearly polarized pump, or nonreciprocal for a circularly polarized pump ($\mathcal{S}_{HV}=-\mathcal{S}_{VH}$), inducing birefringence and Faraday rotation, respectively. The amplitudes of the co- and cross-polarized reflected fields are the same for both pumps, so (d),(e) apply to both (a),(b). For these and later plots, $\Gamma_m=\Omega_m/5000$ and $\kappa=\kappa_c=\Omega_m/10$.

horizontal and vertical polarization axes, respectively), interacting with a localized mechanical mode, with frequency Ω_m, damping constant Γ_m, and annihilation operator $\hat{b}$. We first consider the end-coupled geometry shown in Fig. 1, consisting of a highly reflecting movable mirror that supports a mechanical mode and a partially transparent input-output port. The resonator, assumed to satisfy the resolved sideband condition ($\kappa \ll \Omega_m$), is driven by a red-detuned control field, characterized by the steady-state Jones vector $\bar{\boldsymbol{\alpha}}^T=(\bar{\alpha}_H,\bar{\alpha}_V)$ at a frequency $\omega_L=\tilde{\Delta}+\tilde{\omega}_{\rm cav}$. Here $\tilde{\omega}_{\rm cav}$ includes a static blueshift proportional to the average radiation pressure force $\bar{F}\propto g_0|\bar{\boldsymbol{\alpha}}|^2$. In a frame rotating at red-detuned frequency ω_L ($\tilde{\Delta}=-\Omega_m$), the photons associated with the "probe" fields in sidebands of the stronger control field, denoted by $\delta\hat{\mathbf{a}}\simeq\hat{\mathbf{a}}-\bar{\boldsymbol{\alpha}}$, excite maximally the mechanical mode. The coherent dynamics is thus governed by the linearized Hamiltonian within the rotating-wave approximation (setting $\hbar=1$),

$$\hat{H}_{\rm eff}=-\tilde{\Delta}\delta\hat{\mathbf{a}}^\dagger\delta\hat{\mathbf{a}}+\Omega_m\hat{b}^\dagger\hat{b}-g_0(\bar{\boldsymbol{\alpha}}\cdot\delta\hat{\mathbf{a}}^\dagger\hat{b}+\text{H.c.}), \quad (1)$$

where g_0 denotes the vacuum optomechanical coupling. In a way similar to conversion between photonic modes with different wavelengths [21–23], the synthetic optomechanical interaction in Eq. (1) implements a complex parametric coupling between polarization-orthogonal photons that are degenerate. Essentially, a photon in mode H can be annihilated to produce a phonon in the mechanical resonator, which can subsequently be annihilated to produce a photon in mode V (and vice versa). As we demonstrate below, this enables full spanning of the Poincaré sphere (PS) with the output reflected from a single resonator.

To characterize our system, we obtain the semiclassical equations of motion derived from the coherent evolution Eq. (1) after including dissipation, which for the photonic modes are split into in-coupling and intrinsic loss rates, $\{\kappa_c,\kappa_i\}$ ($\kappa=\kappa_c+\kappa_i$). We define the probe frequency ω in the rotating frame centered on ω_L [see Fig. 1(c)]. The solution for $\hat{b}(\omega)$ is readily found in Fourier space and reinserted into the photonic evolution, yielding the linear system $i\omega\delta\hat{\mathbf{a}}(\omega)=i\mathcal{M}(\bar{\boldsymbol{\alpha}})\delta\hat{\mathbf{a}}(\omega)+\sqrt{\kappa_c}\mathbf{s}_{\rm in}$, where $\mathbf{s}_{\rm in}$ contains probe modes. The 2×2 scattering matrix linking input to output modes ($\mathbf{s}_{\rm out}=\mathcal{S}\mathbf{s}_{\rm in}$) reads [51]

$$\mathcal{S}(\omega,\bar{\boldsymbol{\alpha}})=-\mathbf{1}+i\kappa_c[\mathcal{M}(\bar{\boldsymbol{\alpha}})+\omega\mathbf{1}]^{-1}, \quad (2)$$

where direct reflection is included via the first term and $\mathbf{1}=\text{diag}(1,1)$. In the following, we employ the cooperativity $\mathcal{C}=4g_0^2|\bar{\boldsymbol{\alpha}}|^2/(\Gamma_m\kappa)$ as a relevant figure of merit for the optomechanical system. Further details of the derivation and the resulting $\mathcal{S}$ matrix can be found in Supplemental Material [52].

We explore first the case of linear incident polarization with a finite angle with respect to a linearly polarized control field. The reflectivity spectra for the co- and cross-polarized components of $\mathbf{s}_{\rm in}\|\mathbf{e}_H$, given by $\mathcal{S}_{HH}$ and $\mathcal{S}_{VH}$, respectively, are displayed in Figs. 1(d) and 1(e) for the case $\bar{\boldsymbol{\alpha}}\|\mathbf{e}_{45^\circ}=(\mathbf{e}_H+\mathbf{e}_V)/\sqrt{2}$. The control field thus explicitly breaks rotational symmetry and produces an optomechanically induced mixture of otherwise uncoupled orthogonal polarizations, channeled by a narrow-band mechanical resonance [with effective linewidth $(\mathcal{C}+1)\Gamma_m$]. This phenomenon, emulating a power-controlled birefringence, is characterized by the resonant scattering parameters which depend only on the mechanics via $\mathcal{C}$:

$$\mathcal{S}_{HH}(\Omega_m,\bar{\boldsymbol{\alpha}}\|\mathbf{e}_{45^\circ})=\frac{\kappa_c-(\mathcal{C}+1)\kappa_i}{(\kappa_c+\kappa_i)(\mathcal{C}+1)}, \quad (3a)$$

$$\mathcal{S}_{VH}(\Omega_m,\bar{\boldsymbol{\alpha}}\|\mathbf{e}_{45^\circ})=\frac{\mathcal{C}\kappa_c}{(\kappa_c+\kappa_i)(\mathcal{C}+1)}. \quad (3b)$$

With an increasing driving intensity, the peak and the bandwidth of the conversion are augmented. This efficiency saturates in the large cooperativity limit ($\mathcal{C}\gg1$) at $|\mathcal{S}_{VH}|^2\simeq\kappa_c^2/(\kappa_c+\kappa_i)^2$ and becomes unitary ($|\mathcal{S}_{HH}|^2=0$, $|\mathcal{S}_{VH}|^2=1$) for negligible optical losses $\kappa_i\ll\kappa_c$. A critical aspect in maximizing the conversion efficiency of this process at larger powers is the fulfillment of the sideband-resolved condition, which for fixed detuning ultimately

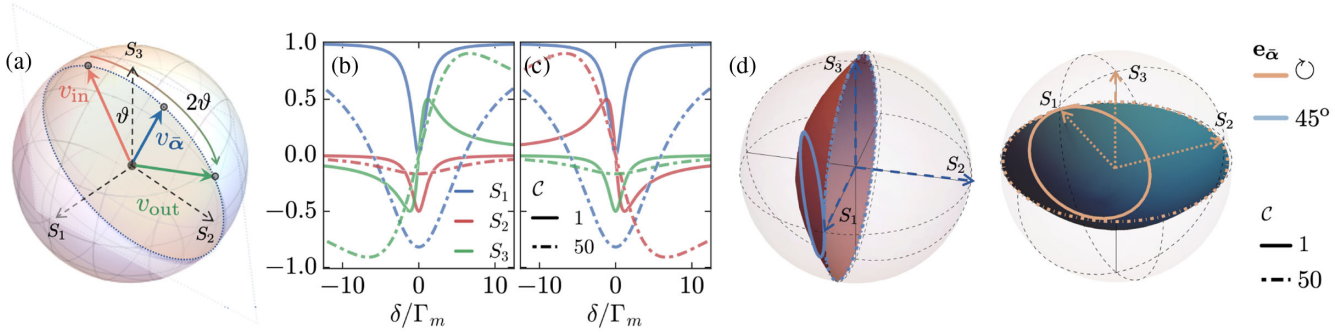

FIG. 2. (a) Illustration of the geometrical transformation induced in the PS by the scattering matrix in Eq. (2). (b)–(d) Stokes parameters for H-polarized incident light and varying input frequency with $\mathcal{C} = 1$ (dashed lines) and $\mathcal{C} = 50$ (solid lines) when the pump is linearly polarized at 45° (b) or right-handed circularly polarized (c). The surface of the sphere can be reached in the limit $\mathcal{C} \gg 1$, but, even at the moderate levels shown here, the output state can nearly be in five of the six Stokes basis states, at the expense of photon losses. (d) Manifolds showing output states for varying cooperativity and detuning [$\delta \in (-\infty, \infty)$] for a linearly polarized pump along 45° (left) and right-handed circular polarization (right). The paths inside the PS for fixed $\mathcal{C} = \{1, 50\}$ are mapped out, with different pump power and polarization, corresponding to (b) and (c). For (b)–(d), other parameters are chosen according to Fig. 1.

limits the bandwidth via $\tilde{\omega}_{\rm cav} - \omega_{\rm cav} < \kappa$. The cavity linewidth itself also imposes the bound $|\omega - \tilde{\omega}_{\rm cav}| < \kappa$.

As revealed by the interaction Hamiltonian in Eq. (1), the mechanical mode selectively couples with the superposition of photonic modes $\bar{\boldsymbol{\alpha}} \cdot \delta\hat{\mathbf{a}}$. The conversion into orthogonal modes $\sim\bar{\boldsymbol{\alpha}}'\delta\hat{\mathbf{a}}$, where $\langle\bar{\boldsymbol{\alpha}}, \bar{\boldsymbol{\alpha}}'\rangle = 0$, is then unaffected by optomechanics, and only a shift in the cavity resonance is expected. For the same control field assumption as above, the scattering matrix elements for parallel and orthogonal conversion channels,

$$\mathcal{S}_{45°H}(\Omega_m, \bar{\boldsymbol{\alpha}} \| \mathbf{e}_{45°}) = -\frac{(\mathcal{C}-1)\kappa_c + (\mathcal{C}+1)\kappa_i}{\sqrt{2}(\kappa_c + \kappa_i)(\mathcal{C}+1)}, \tag{4a}$$

$$\mathcal{S}_{-45°H}(\Omega_m, \bar{\boldsymbol{\alpha}} \| \mathbf{e}_{45°}) = \frac{\kappa_c - \kappa_i}{\sqrt{2}(\kappa_c + \kappa_i)}, \tag{4b}$$

demonstrate this exact phenomena. Only the probe component copolarized with the pump exhibits optomechanically induced transparency or absorption, depending on κ_i, recognized in Ref. [35]. In the limit of low loss and high $\mathcal{C}$, this component undergoes a π phase shift, resulting in strong polarization conversion.

In our system, the conversion of polarization states not only depends on the control intensities, determining the absolute magnitude of the coupling constant in Eq. (1), but is also controlled by the pump phases $\arg(\bar{\alpha}_{H,V})$. The potential of this phase manipulation is uncovered by considering the case of right-handed and left-handed circular polarizations (RHCP and LHCP, respectively), given by $\{\mathbf{e}_{\circlearrowright} = (\mathbf{e}_H + i\mathbf{e}_V)/\sqrt{2}, \mathbf{e}^*_{\circlearrowleft} = \mathbf{e}_{\circlearrowright}\}$ independent of the propagation direction to avoid confusion upon reflection. With a fixed gauge $\arg(\bar{\alpha}_H \bar{\alpha}^*_V) = -\pi/2$, it is straightforward to check that the conversion efficiencies of the H-input probe into the circular bases are equivalent to the conversion into the ±45° bases under linear pumps [Eq. (4)], i.e., $\mathcal{S}_{\circlearrowright H(\circlearrowleft H)}(\bar{\boldsymbol{\alpha}} \| \mathbf{e}_{\circlearrowright}) = \mathcal{S}_{45°H(-45°H)}(\bar{\boldsymbol{\alpha}} \| \mathbf{e}_{45°})$.

Hence, by tailoring the static radiation pressure in a Fabry-Perót cavity, optomechanical interactions permit us to leverage independently the amplitude and phase of the four $\mathcal{S}$-matrix elements, enabling arbitrary polarization control. The relations fulfilled by conversion efficiencies for parallel or orthogonal modes with respect to the control field suggest a geometrical interpretation for the parametric action of the $\mathcal{S}$ matrix. Namely, at large cooperativities, a basis-independent expression for the resonant $\mathcal{S}$ matrix shows conversion insensitive to the mechanical degree of freedom (d.o.f.) (encoded in Γ_m, g_0), namely, $\mathcal{S}(\Omega_m, \bar{\boldsymbol{\alpha}})\mathbf{s}_{\rm in} \simeq -\mathbf{s}_{\rm in} + 2\kappa_c(\mathbf{s}_{\rm in} - \langle\mathbf{e}_{\bar{\boldsymbol{\alpha}}}, \mathbf{s}_{\rm in}\rangle\mathbf{e}_{\bar{\boldsymbol{\alpha}}})/\kappa$, with the control polarization vector $\mathbf{e}_{\bar{\boldsymbol{\alpha}}} = \bar{\boldsymbol{\alpha}}/|\bar{\boldsymbol{\alpha}}|$ playing the role of a (complex) reflection axis for $\mathbf{s}_{\rm in}$ (see [52] for further details). To gain a deeper insight, we use the natural representation of polarization states in the Poincaré sphere that displays the Stokes parameters (S_0, S_1, S_2, S_3), representing the degree of polarization along the bases $\{\mathbf{e}_H, \mathbf{e}_V\}, \{\mathbf{e}_{+45}, \mathbf{e}_{-45}\}$, and $\{\mathbf{e}_{\circlearrowleft}, \mathbf{e}_{\circlearrowright}\}$ [56]. Setting $S_0^{\rm in} = 1$ at the PS surface, the input Jones vector $\mathbf{s}_{\rm in} = (\cos(\theta_{\rm in}/2), e^{i\varphi_{\rm in}}\sin(\theta_{\rm in}/2))$ is thus represented as the Stokes 3-vector $\mathbf{v}_{\rm in} = (\cos(\theta_{\rm in})\sin(\varphi_{\rm in}), \sin(\theta_{\rm in})\sin(\varphi_{\rm in}), \cos(\varphi_{\rm in}))$, while the $\mathcal{S}$ mapping induces a reflection of $\mathbf{v}_{\rm in}$ over the parametric axis along the control vector $\mathbf{v}_{\bar{\boldsymbol{\alpha}}}$ for an overcoupled resonator ($\kappa_i \ll \kappa_c$), namely, $\mathbf{v}_{\rm out} \simeq 2(\mathbf{v}_{\bar{\boldsymbol{\alpha}}} \cdot \mathbf{v}_{\rm in})\mathbf{v}_{\bar{\boldsymbol{\alpha}}} - \mathbf{v}_{\rm in}$ [57]. The whole surface of the PS can therefore be spanned by rotating $\mathbf{e}_{\bar{\boldsymbol{\alpha}}}$ [see Fig. 2(a)].

We next explore how driving frequencies can be exploited as an additional d.o.f. in the conversion process, beyond constraints imposed by the active control of driving polarization. For instance, when the probe frequency matches the optical resonance, a finite detuning of the control field (denoted by $\delta = \Omega_m - \omega_L$) alters the response of the signal component parallel to the pump. To see to

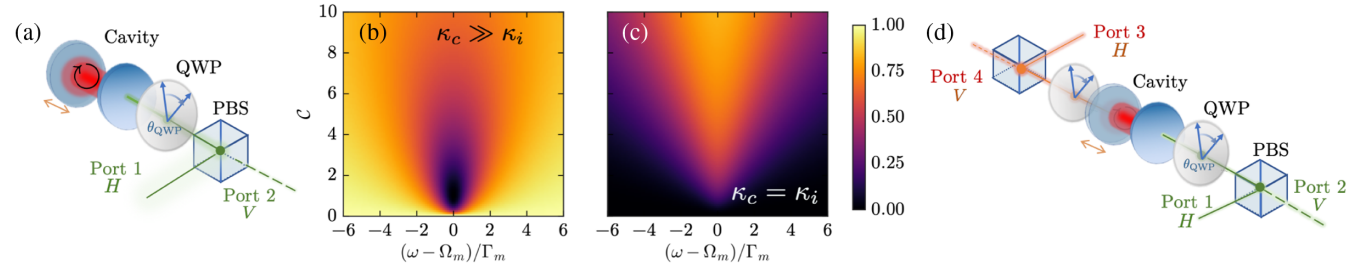

FIG. 3. (a) Schematic for the realization of a free-space optical isolator. (b) Transmission $|\mathcal{S}_{VH}|^2$ for the overcoupled case, where $|\mathcal{S}_{HV}| \simeq 1$. Good isolation occurs for $\mathcal{C} \simeq 1$ and over the mechanical linewidth, where losses through the mechanical mode can occur. (c) Transmission $|\mathcal{S}_{VH}|^2$ for the critically coupled case. With larger pumping, the transmission amplitude and bandwidth both increase. (d) Schematic for a potential implementation as a four-port circulator. For (b),(c), other parameters are chosen according to Fig. 1.

what extent the polarization is affected, Fig. 2(b) shows the Stokes parameters for the reflection from a cavity probed by H-polarized light, with an LP control field along 45°. Recovering previous results, we observe full dissipation of the copolarized probe component into the mechanical mode at resonance ($\delta = 0$) for an overcoupled resonator ($\kappa_i \ll \kappa_c$) driven at moderate cooperativities ($\mathcal{C} \sim 1$). The system then behaves as a conventional polarizing mirror, reflecting only light cross-polarized to the control. Similar physics is observed for an RHCP control in Fig. 2(c), where the reflection is purely LHCP ($S_3 < 0$). Efficient conversion into the polarization state $\mathbf{e}_V$, sitting at $S_1 = -1$, is recovered at $\mathcal{C} \gg 1$ for both cases. For large cooperativity, the component parallel to the pump is entirely reflected, but with a phase that spans from 0 to 2π relative to the orthogonal component as the detuning is varied (see [52]), resulting in a conversion into elliptic polarization ($S_{1,2,3} \neq 0$). We note here that the conservation of energy and angular momentum for modes undergoing conversion must be met by slight changes to the control beam, which we have neglected in the linearized, strong pump approximation.

Furthermore, within the geometrical argument presented in Fig. 2(a), finite detuning results in output Stokes vectors with a component orthogonal to the control plane leading to extra control over the output polarization beyond resonant conversion. In order to benchmark this approach, we trace in Fig. 2(d) the manifold of reachable Stokes parameters on the PS as δ is swept across the range $\delta \in (-\infty, \infty)$ and the cooperativity is increased above zero, i.e., $\mathcal{C} > 0$, for the 45° and RHCP control polarizations (left or right panels). The loci of output states form bowl-shaped surfaces that emerge from the zero-conversion point at $S_1 = 1$ (state $\mathbf{e}_H$) for $\mathcal{C} = 0$ and infiltrate the PS for intermediate $\mathcal{C}$. In particular, at a fixed cooperativity, the output states follow circular orbits with radii growing with $\mathcal{C}$. The output reaches the state $\mathbf{e}_V$ at the (antipodal) location $S_1 = -1$, obtained by reflecting the input across the parametric control plane in the limit $\mathcal{C} \gg 1$ and resonance ($\delta = 0$), recovering previous results. From a global perspective, the Stokes vector of a strong control field serves as an axis of rotation for an arbitrary probe field as the frequency is varied, with a maximum 180° rotation for $\delta = 0$, as in Fig. 2(a). In this fashion, it is feasible to reach four out of the six poles of the PS along the axes $S_{1,2,3}$ by just varying detuning. An extra fifth pole of the PS is reached at the expense of losses in the polarizer operation. This demonstrates the potential of this system as a reconfigurable efficient polarization generator.

Interestingly, finite ellipticity of the control field induces conversion processes that are nonreciprocal in nature. In the case of circular polarization, the scattering matrix is antisymmetric, signaling the breaking of Lorentz reciprocity ($\mathcal{S} = -\mathcal{S}^T \neq \mathcal{S}^T$; see Supplemental Material [52]). Antisymmetry of the scattering matrix is inherited from the complex phase $\arg(\bar{\alpha}_H^* \bar{\alpha}_V)$ imprinted by the control field at the level of the interaction Hamiltonian in Eq. (1). Such features show time-reversal symmetry breaking and (nonreciprocal) Faraday rotation in the system and result in the inability to relate forward or backward scattering transformations [57].

Phase nonreciprocity can be readily exploited to build devices displaying unconventional photon routing [58], such as an optical isolator, where the off-diagonal transmission coefficients have unequal amplitudes. A possible approach consists in placing a suitably oriented quarter-wave plate (QWP) after the output mirror of a CP-driven resonator (without loss of generality RHCP) in addition to a polarizing beam splitter (PBS), forming the ports sketched in Fig. 3(a). Then, an H-polarized input probe (port 1) is reflected in the PBS and acquires an RHCP component upon passing the QWP. This component yields a V-polarized output (port 2), after a second pass through the QWP, with a transmission level tunable by interactions with the mechanical mode. Following a similar logic, a V-polarized probe in port 2 is insensitive to the mechanics and has a fixed transmission to port 1. In this system, losses, inherently required by a linear two-port isolator [59], are found in preferential absorption of one of the CP components.

This is confirmed by a quantitative analysis of the device action on the input, characterized by $\mathcal{S}_{\text{iso}} = \mathcal{A}_{\text{QWP}} \mathcal{S} \mathcal{A}_{\text{QWP}}$, where $\mathcal{A}_{\text{QWP}} = (1/\sqrt{2})(\mathbf{1} + i\sigma_x)$ and $\mathcal{S}$ follows from

Eq. (2). For illustrative purposes, we consider two limiting scenarios, in which the optical cavity is either (i) overcoupled ($\kappa_i \ll \kappa_c$) or (ii) critically coupled ($\kappa_i = \kappa_c$) [51]. If the control field in the resonator is set to RHCP, then in the former case, the RHCP probe can be absorbed through the mechanical modes with moderate cooperativities, leading to vanishing reflected output, i.e., $\mathcal{S}_{VH} \simeq 0$ [see Fig. 3(b)]. Meanwhile, the LHCP light will not interact with the mechanical mode and will be reflected independent of cooperativity ($|\mathcal{S}_{HV}| \simeq 1$). Efficient isolation occurs for $\mathcal{C} = 1$ over a narrow bandwidth limited by the mechanical resonance, Γ_m. For critical coupling, light is absorbed without interacting with the mechanical mode for low $\mathcal{C}$ [$\mathcal{S} \simeq \mathbf{0}$ in Fig. 3(c)]. In this case, $\mathcal{S}_{VH}$ exhibits features reminiscent from optomechanically induced transparency, with an increasing efficiency and bandwidth for large cooperativities, similar to polarization conversion in the overcoupled cavity displayed in Fig. 1(d), while $\mathcal{S}_{HV} \simeq 0$ regardless of the pump power. Arbitrary contributions of κ_c and κ_i yield a behavior interpolating between the two limits above.

If the reflectivity of the second mirror is decreased below unity, so light entering in the resonator can outcouple to the other side, the addition of the same QWP-PBS plate to this side, as sketched in Fig. 3(c), permits nonreciprocal light circulation between a port i and a port $i+1$, for $i = \{1, 2, 3, 4\}$. This setup is precisely mappable into an optomechanically assisted four-port optical circulator [31]. A benchmark of this device can be found in Supplemental Material [52].

In conclusion, we have demonstrated how a minimal setup, consisting of an optomechanical cavity in the resolved-sideband regime, is a versatile platform for all-optical polarization conversion. Parametric photon-phonon interactions induce birefringence for a probe beam in a rotationally symmetric system. Our results then highlight how the freedom in both vectorial (polarization) and scalar (intensity and frequency) d.o.f. in the incoming fields can be exploited to achieve arbitrary polarization states in reflection. In particular, we have shown how birefringence is expected for linearly polarized control beams, and, similarly, nonreciprocal Faraday rotation can be realized for circular polarization. Finally, the design of an optical isolator based upon this configuration is presented, showing the requirements and tradeoffs that would exist in a realistic implementation of such a system. These concepts may be straightforwardly extended to other settings supporting degenerate optomechanical resonances, including potentially integrated platforms, or by exploiting stimulated Brillouin scattering in polarization-degenerate waveguides or fibers [60,61]. Even more opportunities might arise when many mechanical modes are engaged, allowing more complex polarization manipulations, or via optomechanical amplification at $\tilde{\Delta} = \Omega_m$, boosting conversion efficiency and enabling directional amplification. Our findings altogether unlock a new potential of optomechanics in manipulating light fields by interfacing with mechanical d.o.f., enabling unusual reciprocal and nonreciprocal phenomena for polarization conversion and manipulation.

E. V. thanks Frank Buters, whose thesis defense inspired thinking about the proposed concepts. The authors acknowledge support from the Office of Naval Research (Grants No. N00014-19-1-2011 and No. 014-16-1-2466) and the Air Force Office of Scientific Research with MURI Grant No. FA9550-18-1-0379. This work is part of the research program of the Netherlands Organisation for Scientific Research (NWO). It is furthermore supported by the European Research Council (ERC Starting Grant No. 759644-TOPP) and the European Union's Horizon 2020 research and innovation program under Grant Agreement No. 732894 (FET Proactive HOT).

*These authors contributed equally to this work.
†aalu@gc.cuny.edu

[1] M. A. Nielsen and I. L. Chuang, *Quantum Computation and Quantum Information* (Cambridge University Press, Cambridge, England, 2010).
[2] W. Xiong, C. W. Hsu, Y. Bromberg, J. E. Antonio-Lopez, R. Amezcua Correa, and H. Cao, Complete polarization control in multimode fibers with polarization and mode coupling, Light Sci. Appl. **7**, 54 (2018).
[3] S. Inoue, Video image processing greatly enhances contrast, quality, and speed in polarization-based microscopy, J. Cell Biol. **89**, 346 (1981).
[4] J. F. de Boer, T. E. Milner, M. J. C. van Gemert, and J. S. Nelson, Two-dimensional birefringence imaging in biological tissue by polarization-sensitive optical coherence tomography, Opt. Lett. **22**, 934 (1997).
[5] Y. Zhao and A. Alù, Manipulating light polarization with ultrathin plasmonic metasurfaces, Phys. Rev. B **84**, 205428 (2011).
[6] C. Pfeiffer, C. Zhang, V. Ray, L. Jay Guo, and A. Grbic, Polarization rotation with ultra-thin bianisotropic metasurfaces, Optica **3**, 427 (2016).
[7] N. K. Grady, J. E. Heyes, D. R. Chowdhury, Y. Zeng, M. T. Reiten, A. K. Azad, A. J. Taylor, D. A. R. Dalvit, and H. T. Chen, Terahertz metamaterials for linear polarization conversion and anomalous refraction, Science **340**, 1304 (2013).
[8] A. Arbabi, Y. Horie, M. Bagheri, and A. Faraon, Dielectric metasurfaces for complete control of phase and polarization with subwavelength spatial resolution and high transmission, Nat. Nanotechnol. **10**, 937 (2015).
[9] Z. Wu, Y. Ra'di, and A. Grbic, Tunable Metasurfaces: A Polarization Rotator Design, Phys. Rev. X **9**, 011036 (2019).
[10] D. Floess, J. Y. Chin, A. Kawatani, D. Dregely, H.-U. Habermeier, T. Weiss, and H. Giessen, Tunable and switchable polarization rotation with non-reciprocal plasmonic thin films at designated wavelengths, Light Sci. Appl. **4**, e284 (2015).

[11] A. Fallahi and J. Perruisseau-Carrier, Manipulation of giant Faraday rotation in graphene metasurfaces, Appl. Phys. Lett. **101**, 231605 (2012).
[12] F. J. Rodríguez-Fortuño, D. Puerto, A. Griol, L. Bellieres, J. Martí, and A. Martínez, Universal method for the synthesis of arbitrary polarization states radiated by a nanoantenna, Laser Photonics Rev. **8**, L27 (2014).
[13] A. She and F. Capasso, Parallel polarization state generation, Sci. Rep. **6**, 26019 (2016).
[14] A. H. Safavi-Naeini and O. Painter, Proposal for an optomechanical traveling wave phonon-photon translator, New J. Phys. **13**, 013017 (2011).
[15] V. Fiore, Y. Yang, M. C. Kuzyk, R. Barbour, L. Tian, and H. Wang, Storing Optical Information as a Mechanical Excitation in a Silica Optomechanical Resonator, Phys. Rev. Lett. **107**, 133601 (2011).
[16] E. Verhagen, S. Deléglise, S. Weis, A. Schliesser, and T. J. Kippenberg, Quantum-coherent coupling of a mechanical oscillator to an optical cavity mode, Nature (London) **482**, 63 (2012).
[17] T. A. Palomaki, J. W. Harlow, J. D. Teufel, R. W. Simmonds, and K. W. Lehnert, Coherent state transfer between itinerant microwave fields and a mechanical oscillator, Nature (London) **495**, 210 (2013).
[18] S. Weis, R. Rivière, S. Deléglise, E. Gavartin, O. Arcizet, A. Schliesser, and T. J. Kippenberg, Optomechanically induced transparency, Science **330**, 1520 (2010).
[19] A. H. Safavi-Naeini, T. P. Mayer Alegre, J. Chan, M. Eichenfield, M. Winger, Q. Lin, J. T. Hill, D. E. Chang, and O. Painter, Electromagnetically induced transparency and slow light with optomechanics, Nature (London) **472**, 69 (2011).
[20] C. A. Regal and K. W. Lehnert, From cavity electromechanics to cavity optomechanics, J. Phys. Conf. Ser. **264**, 012025 (2011).
[21] C. Dong, V. Fiore, M. C. Kuzyk, and H. Wang, Optomechanical dark mode, Science **338**, 1609 (2012).
[22] J. T. Hill, A. H. Safavi-Naeini, J. Chan, and O. Painter, Coherent optical wavelength conversion via cavity optomechanics, Nat. Commun. **3**, 1196 (2012).
[23] R. W. Andrews, R. W. Peterson, T. P. Purdy, K. Cicak, R. W. Simmonds, C. A. Regal, and K. W. Lehnert, Bidirectional and efficient conversion between microwave and optical light, Nat. Phys. **10**, 321 (2014).
[24] L. Tian and H. Wang, Optical wavelength conversion of quantum states with optomechanics, Phys. Rev. A **82**, 053806 (2010).
[25] L. Tian, Adiabatic State Conversion and Pulse Transmission in Optomechanical Systems, Phys. Rev. Lett. **108**, 153604 (2012).
[26] D. Lee, M. Underwood, D. Mason, A. B. Shkarin, S. W. Hoch, and J. G. E. Harris, Multimode optomechanical dynamics in a cavity with avoided crossings, Nat. Commun. **6**, 6232 (2015).
[27] Y.-D. Wang and A. A. Clerk, Reservoir-Engineered Entanglement in Optomechanical Systems, Phys. Rev. Lett. **110**, 253601 (2013).
[28] Y.-D. Wang, S. Chesi, and A. A. Clerk, Bipartite and tripartite output entanglement in three-mode optomechanical systems, Phys. Rev. A **91**, 013807 (2015).
[29] M. C. Kuzyk, S. J. van Enk, and H. Wang, Generating robust optical entanglement in weak-coupling optomechanical systems, Phys. Rev. A **88**, 062341 (2013).
[30] Z. Shen, Y.-L. Lei Zhang, Y. Chen, C.-L. Zou, Y.-F. Xiao, X.-B. Zou, F.-W. Sun, G.-C. Guo, and C.-H. Dong, Experimental realization of optomechanically induced non-reciprocity, Nat. Photonics **10**, 657 (2016).
[31] F. Ruesink, M.-A. Miri, A. Alù, and E. Verhagen, Nonreciprocity and magnetic-free isolation based on optomechanical interactions, Nat. Commun. **7**, 13662 (2016).
[32] K. Fang, J. Luo, A. Metelmann, M. H. Matheny, F. Marquardt, A. A. Clerk, and O. Painter, Generalized non-reciprocity in an optomechanical circuit via synthetic magnetism and reservoir engineering, Nat. Phys. **13**, 465 (2017).
[33] G. A. Peterson, F. Lecocq, K. Cicak, R. W. Simmonds, J. Aumentado, and J. D. Teufel, Demonstration of Efficient Nonreciprocity in a Microwave Optomechanical Circuit, Phys. Rev. X **7**, 031001 (2017).
[34] F. Ruesink, J. P. Mathew, M.-A. Miri, A. Alù, and E. Verhagen, Optical circulation in a multimode optomechanical resonator, Nat. Commun. **9**, 1798 (2018).
[35] H. Xiong, Y. M. Huang, L. L. Wan, and Y. Wu, Vector cavity optomechanics in the parameter configuration of optomechanically induced transparency, Phys. Rev. A **94**, 013816 (2016).
[36] F. M. Buters, M. J. Weaver, H. J. Eerkens, K. Heeck, S. de Man, and D. Bouwmeester, Optomechanics with a polarization nondegenerate cavity, Phys. Rev. A **94**, 063813 (2016).
[37] S. Zanotto, A. Tredicucci, D. Navarro-Urrios, M. Cecchini, G. Biasiol, D. Mencarelli, L. Pierantoni, and A. Pitanti, Optomechanics of chiral dielectric metasurfaces, arXiv: 1810.01773.
[38] A. Abramovici, W. E. Althouse, R. W. P. Drever, Y. Gürsel, S. Kawamura, F. J. Raab, D. Shoemaker, L. Sievers, R. E. Spero, K. S. Thorne, R. E. Vogt, R. Weiss, S. E. Whitcomb, and M. E. Zucker, LIGO: The laser interferometer gravitational-wave observatory, Science **256**, 325 (1992).
[39] P. F. Cohadon, A. Heidmann, and M. Pinard, Cooling of a Mirror by Radiation Pressure, Phys. Rev. Lett. **83**, 3174 (1999).
[40] T. Corbitt, D. Ottaway, E. Innerhofer, J. Pelc, and N. Mavalvala, Measurement of radiation-pressure-induced optomechanical dynamics in a suspended Fabry-Perot cavity, Phys. Rev. A **74**, 021802(R) (2006).
[41] J. D. Thompson, B. M. Zwickl, A. M. Jayich, Florian Marquardt, S. M. Girvin, and J. G. E. Harris, Strong dispersive coupling of a high finesse cavity to a micromechanical membrane, Nature (London) **452**, 72 (2008).
[42] I. Favero, S. Stapfner, D. Hunger, P. Paulitschke, J. Reichel, H. Lorenz, E. M. Weig, and K. Karrai, Fluctuating nanomechanical system in a high finesse optical microcavity, Opt. Express **17**, 12813 (2009).
[43] S. Gröblacher, K. Hammerer, M. R. Vanner, and M. Aspelmeyer, Observation of strong coupling between a micromechanical resonator and an optical cavity field, Nature (London) **460**, 724 (2009).
[44] T. P. Purdy, R. W. Peterson, P.-L. Yu, and C. A. Regal, Cavity optomechanics with Si_3N_4 membranes at cryogenic temperatures, New J. Phys. **14**, 115021 (2012).

[45] M. Karuza, C. Molinelli, M. Galassi, C. Biancofiore, R. Natali, P. Tombesi, G. Di Giuseppe, and D. Vitali, Optomechanical sideband cooling of a thin membrane within a cavity, New J. Phys. **14**, 095015 (2012).

[46] S. Anguiano, A. E. Bruchhausen, B. Jusserand, I. Favero, F. R. Lamberti, L. Lanco, I. Sagnes, A. Lemaître, N. D. Lanzillotti-Kimura, P. Senellart, and A. Fainstein, Micropillar Resonators for Optomechanics in the Extremely High 19–95-GHz Frequency Range, Phys. Rev. Lett. **118**, 263901 (2017).

[47] M. Rossi, D. Mason, J. Chen, Y. Tsaturyan, and A. Schliesser, Measurement-based quantum control of mechanical motion, Nature (London) **563**, 53 (2018).

[48] P. Kharel, G. I. Harris, E. A. Kittlaus, W. H. Renninger, N. T. Otterstrom, J. G. E. Harris, and P. T. Rakich, High-frequency cavity optomechanics using bulk acoustic phonons, Sci. Adv. **5**, eaav0582 (2019).

[49] M. Liu, D. A. Powell, R. Guo, I. V. Shadrivov, and Y. S. Kivshar, Polarization-induced chirality in metamaterials via optomechanical interaction, Adv. Opt. Mater. **5**, 1600760 (2017).

[50] S. Wielandy and A. L. Gaeta, Coherent Control of the Polarization of an Optical Field, Phys. Rev. Lett. **81**, 3359 (1998).

[51] M.-A. Miri, F. Ruesink, E. Verhagen, and A. Alù, Optical Nonreciprocity Based on Optomechanical Coupling, Phys. Rev. Applied **7**, 064014 (2017).

[52] See Supplemental Material at http://link.aps.org/supplemental/10.1103/PhysRevLett.123.023602 for a detailed derivation of the scattering matrix, the geometrical scattering description in the high cooperativity limit, and a further discussion of circulator operation, which includes Refs. [53–55].

[53] R. W. Brockett, Robotic manipulators and the product of exponentials formula, in *Mathematical Theory of Networks and Systems*, edited by P. A. Fuhrmann, Lecture Notes in Control and Information Sciences Vol. 58 (Springer, Berlin, Heidelberg, 1984).

[54] W. Bowen and G. J. Milburn, *Quantum Optomechanics* (CRC Press, Boca Raton, 2015)

[55] M. S. Bartlett, An inverse matrix adjustment arising in discriminant analysis, Ann. Math. Statist. **22**, 107 (1951).

[56] E. Collett, *Field Guide to Polarization*, Vol. 15 (SPIE Press, Bellingham, 2005).

[57] L. Ranzani and J. Aumentado, A geometric description of nonreciprocity in coupled two-mode systems, New J. Phys. **16**, 103027 (2014).

[58] E. Verhagen and A. Alù, Optomechanical nonreciprocity, Nat. Phys. **13**, 922 (2017).

[59] D. M. Pozar, *Microwave Engineering*, 4th ed. (John Wiley & Sons, Hoboken, NJ, 2012).

[60] M. O. van Deventer and A. J. Boot, Polarization properties of stimulated Brillouin scattering in single-mode fibers, J. Lightwave Technol. **12**, 585 (1994).

[61] I. Aryanfar, C. Wolff, M. J. Steel, B. J. Eggleton, and C. G. Poulton, Mode conversion using stimulated Brillouin scattering in nanophotonic silicon waveguides, Opt. Express **22**, 29270 (2014).